Spinning Black Hole Mergers: A Primer

PHZ6607

Luis Ortega

December 6, 2018

Contents

1 Introduction

The mergers of spinning black holes can create some of the most interesting effects due to the non-linear fields present near them. To understand the complexity in solving the motion and gravitational radiation of spinning black hole mergers, we must look at the simplest configurations first and then add details. We begin by presenting first an introduction to the Kerr metric and the basic properties of spinning black holes, as well as the tools which physicists use to model and understand black hole interactions. With this knowledge, we can

proceed to a survey of the properties of binary black hole mergers and the effects introduced once we consider of spinning black holes as the components of these mergers. It is important that we understand, at least qualitatively, the properties of spinning black hole mergers and the conclusions we can draw from their observation on the formation of these systems.

2 Spinning Black Holes: The Kerr Metric [41]

Soon after Albert Einstein produced the final form of his theory of general relativity, Karl Schwarzschild solved the field equations for the spacetime geometry of a non-spinning point source in vacuum [34]. This solution was extended to model the spacetime geometry outside of any spherical source and later lead to the prediction of non-spinning black holes. From the Schwarzschild metric, came the 'no hair theorem' [16], which states that all black hole solutions can be completely described by the mass, electric charge, and angular momentum parameters. It would take almost half a century before the spacetime metric for a rotating mass would be discovered by Roy Kerr [23]. The angular momentum of the spinning mass breaks spherical symmetry, and makes the calculations much more complex algebraically. The derivation of the Kerr metric is well beyond the scope (and length) of this paper, we present it as in Kerr's original paper

$$\begin{aligned} ds^2 = (r^2 + a^2 cos^2\theta)(d\theta^2 + sin^2\theta d\phi^2) + 2(du + asin^2\theta d\phi)(dr + asin^2\theta d\phi) \\ - \left(1 - \frac{2mr}{r^2 + a^2 cos^2\theta}\right)(du + asin^2\theta d\phi)^2 \end{aligned} \tag{1}$$

where $a = \frac{J}{m}$. Note that, as we might expect, setting a $\to$ 0, this reduces to the Schwarzschild metric

$$ds^2 \to -1\left(1 - \frac{2m}{r}\right)du^2 + 2dudr + r^2(d\theta^2 + sin^2\theta d\phi^2) \tag{2}$$

and setting m $\to$ 0, it reduces to flat Minkowski space in spheroidal polar coordinates (this isn't obvious and the equation isn't illuminating.)
Departing from the Schwarzschild black hole, the Kerr metric has two values of r for which the metric exhibits singularities

$$r = r_\pm = m \pm \sqrt{m^2 - a^2} \tag{3}$$

These represent coordinate singularities of the metric rather than curvature singularities and represent the event horizons. As a $\to$ 0 we see that $r_+ \to 2m$ (and $r_- \to 0m$,) which is the location of the event horizon in Schwarzschild metric.

The Kerr metric also displays a region in which g_{tt} is negative, meaning 't' acts as a spatial component and indicates a lack of a time dimension, given by

$$r = r_E^{\pm} = m \pm \sqrt{m^2 - a^2 cos^2\theta} \tag{4}$$

In this region, time-like or light-like worldlines must co-rotate with the inner mass (nothing can stand still!) This is referred to as frame-dragging (or the Lense-Thirring effect); the spinning black hole drags spacetime around with it. The frame-dragging effect has been tested and confirmed to an accuracy of 1% by NASA's Gravity Probe B Experiment [10]. This effect also leads to other interesting properties, though this paper won't discuss negative energy particle trajectories or the details of energy extraction from a black hole by the Penrose process.

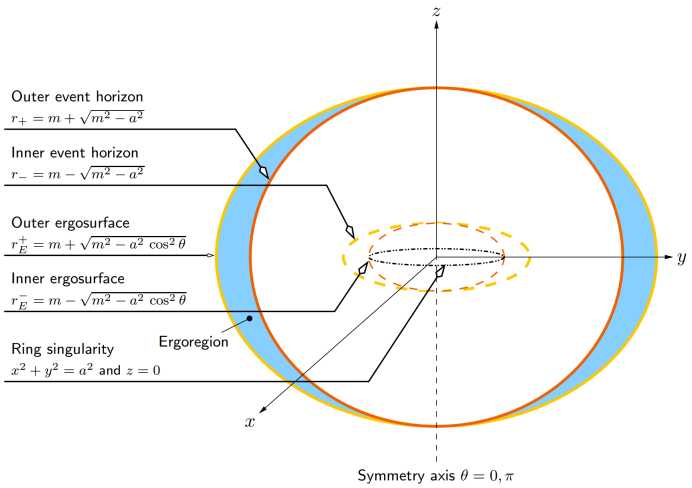

Figure 1: Schematic of important features which arise from the Kerr solution. [41]

The No Hair Theorem states that mass, angular momentum and charge compose a complete parameter set for describing black holes. While theorists consider the existence of charged spinning and non-spinning black holes, astrophysical black holes (the subject of this paper) are likely to be neutral or nearly neutral as a charged black hole would quickly be neutralized by surrounding plasma. We will assume charge to be 0.

3 Approximations in Weak and Strong Fields

Solving Einstein's equations is no easy task, and solving them for two body systems such as the merger of black holes (spinning or not) requires the use of approximation techniques. In this section we will explore the tools used by physicists to find the approximate solution of the field equations in the weak and strong field regimes.

In the inspiral phase of a binary black hole merger, post-Newtonian approximations closely approach the solutions. However, in the non-linear merger phase post-Newtonian approximations will deviate from the expected results. In this regime, numerical relativity

can produce solutions which closely approximate the real solutions. The black hole perturbative quasi-normal modes (QNM) models used to analyze the ring-down phase of the merger provide insight into the final properties of the black coalescence.

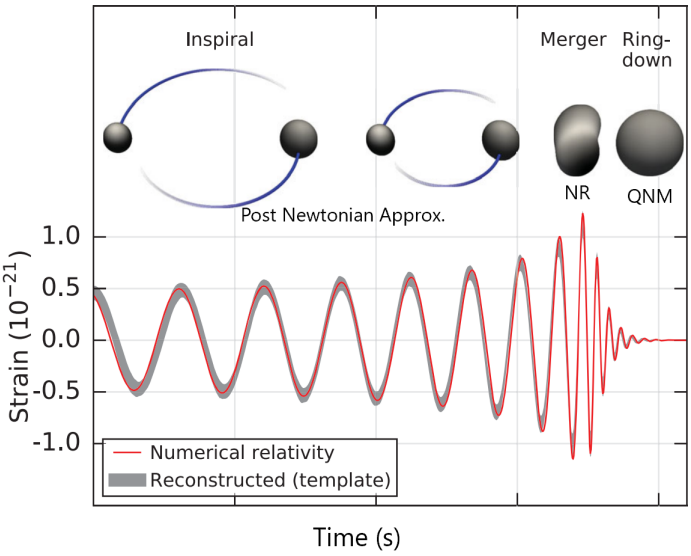

Figure 2: Phases of a binary black hole merger and the approximation techniques used in each (top) and the gravitational waveform created by a merger during the entire progression from inspiral to plung, merger and ringdown (bottom.) [9]

Quasi-normal modes are the modes of energy dissipation of perturbations around a black hole solution; they differ from normal modes in that the system is open and loses energy through the emission of gravitational waves. The quasi-normal modes that show up in the ringdown phase of binary black hole mergers are the characteristic modes of oscillation of a specific spacetime. This means that they don't depend on the behavior leading to them and describe only the newly formed black hole. An approximate solution for the quasi-normal mode freqeuncies of the Kerr black hole is [4]

$$\omega \approx \frac{1}{3\sqrt{3}M}\left[\pm\left(\ell+\frac{1}{2}\right)+\frac{2am}{3\sqrt{3}M}-i\left(n+\frac{1}{2}\right)\right] \tag{5}$$

Here, $\ell \geq m \geq 1$ and $a \leq M$; m is the azimuthal number. Thus, if both the frequency of oscillation and the damping time of the fundamental quasi-normal mode can be detected (which LIGO does) then this equation can be used to obtain the mass M and rotation parameter a of the black hole.

3.1 Post-Newtonian Expansion [31]

Post-Newtonian theory is an approximation to general relativity that holds in the weak field limit. It is useful in modeling binaries because it can be used to model bodies with

strong internal gravity as long as the gravitational interaction between the two bodies is weak as is the case in the inspiral phase.

Post-Newtonian theory starts with the Landau-Lifshitz formulation of general relativity. In this framework, the main variables are not the components of the metric tensor $g_{\alpha\beta}$ but those of the "gothic" metric density $\mathfrak{g}^{\alpha\beta} \equiv \sqrt{-g}g^{\alpha\beta}$. The Einstein field equations are

$$\begin{aligned}
&\partial_{\mu\nu} H^{\alpha\mu\beta\nu} = \frac{16\pi G}{c^4}(-g)(T^{\alpha\beta} + t_{LL}^{\alpha\beta}) \\
&H^{\alpha\mu\beta\nu} = \mathfrak{g}^{\alpha\beta}\mathfrak{g}^{\mu\nu} - \mathfrak{g}^{\alpha\nu}\mathfrak{g}^{\beta\mu} \\
&\text{where} \qquad t_{LL}^{\alpha\beta} \sim \partial\mathfrak{g} \cdot \partial\mathfrak{g} \qquad \text{is the field-energy momentum} \\
&\partial\beta \left[(-g)(T^{\alpha\beta} + t_{LL}^{\alpha\beta})\right] = 0 \rightarrow \nabla_\beta T^{\alpha\beta} = 0 \qquad \text{conservation equation}
\end{aligned} \tag{6}$$

To formulate the approximation scheme, first we define the potential $h^{\alpha\beta} = \eta^{\alpha\beta} - \mathfrak{g}^{\alpha\beta}$ and impose the harmonic gauge condition $\partial_\beta h^{\alpha\beta} = 0$. For which we get the relaxed field equations are

$$\begin{aligned}
&\Box h^{\alpha\beta} = -\frac{16\pi G}{c^4}\tau^{\alpha\beta} \\
&\Box = -\frac{1}{c^2}\frac{\partial^2}{\partial t^2} + \frac{\partial^2}{\partial x^2} + \frac{\partial^2}{\partial y^2} + \frac{\partial^2}{\partial z^2} \\
&\tau^{\alpha\beta} = (-g)(T^{\alpha\beta} + t_{LL}^{\alpha\beta} + t_H^{\alpha\beta}) \\
&t_H^{\alpha\beta} \sim \partial h \cdot \partial h + h\partial^2 h \\
&\partial_\beta \tau^{\alpha\beta} = 0 \rightarrow \partial_\beta h^{\alpha\beta} = 0 \qquad \text{conservation equation}
\end{aligned} \tag{7}$$

Note this is a wave equation in flat spacetime, with a source $\tau^{\alpha\beta}$ constructed from matter and field variables. The full set of Einstein equations are contained in the first equation and the conservation equation; this is still an exact formulation of general relativity. Now we can solve the first equation for $h^{\alpha\beta}$ as a function of a given distribution of matter. The behavior of the matter can be determined by the conservation equation.

The integration of the wave equation is solved in iterations. We assume that $h^{\alpha\beta}$ is small, then

$$\begin{aligned}
&\Box h_{N+1}^{\alpha\beta} = -\frac{16\pi G}{c^4}\tau^{\alpha\beta}(h_N) \\
&h_{N+1}^{\alpha\beta} = \frac{4G}{c^4}\int \frac{\tau^{\alpha\beta}(t - |\mathbf{x} - \mathbf{x}'|/\mathbf{c}, \mathbf{x}')}{|\mathbf{x} - \mathbf{x}'|} d^3x'
\end{aligned} \tag{8}$$

We start the iterations with $h_0^{\alpha\beta} = 0$ and stop at the level of accuracy desired, this is where the process really becomes an approximation. Once $h_N^{\alpha\beta}$ is found, the motion of the

matter is solved using the conservation equation.

Post-Newtonian orders are counted based on orders of v/c. Specifically, a Post-Newtonian correction of order $(v/c)^n$ to a Newtonian expression is of $(n/2)$PN order.

3.2 Numerical Relativity

Solving Einstein's equations analytically in the non-linear strong-field regime proves to be difficult, yet it is necessary to obtain precise solutions to understand theoretical and observational results of binary black hole mergers. In this regime, numerical relativity uses computational methods and algorithms to approximate solutions to Einstein's equations for phenomena whose exact spacetime geometry is not known. Decades of development in algorithms, computational techniques and computational power took place before relatively recent breakthroughs in numerical techniques allowed for this undertaking to begin to realize.

The approach in numerical relativity is to formulate Einstein's equations into a time-step iteration process that would take a set of initial conditions and evolve them through the coalescence until the final state. This computational framework, referred to as the "3+1 approach" because space and time are separated, is a Hamiltonian formulation of of general relativity. It is also referred to as ADM formalism for Arnowitt, Deser and Misner, who first proposed the idea [33].

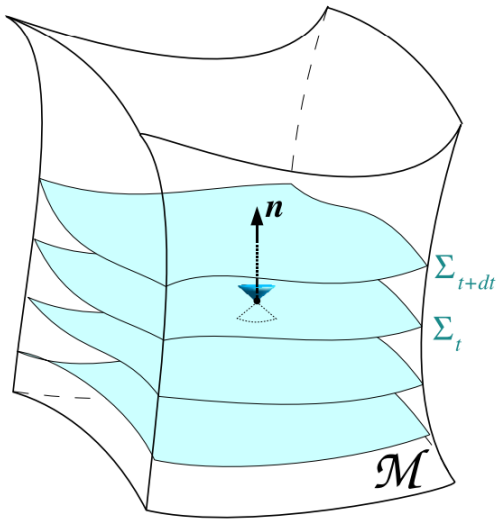

Figure 3: Foliation of a manifold $\mathcal{M}$ [15]

In 3+1 formalism [15], a globally hyperbolic four-dimensional spacetime is sliced into a large number of continuous three-dimensional surfaces (spacelike hypersurfaces called leafs or slices) separated by some time dt; this is the foliation (figure 3). dt composes a smooth scalar

field t which is regular, such that every slice is a level surface and the formed hypersurfaces are non-intersecting. There is a timelike, future directed unit vector normal to each hypersurface,

$$\vec{n} = -N\nabla t \qquad \text{where} \qquad N = (-\nabla t \cdot \nabla t)^{1/2} \tag{9}$$

N (or α) is the lapse function, which determines the time step between slices ($\delta\tau = N(t,x)\delta t$) and is chosen so as to avoid singularities and improve the overall result and speed of the computation. N^i (or β^i) describe the way in which the 3 spatial coordinates change between slices.

With these 4 Lagrange multipliers, the dynamic variables in the 3D metric tensor γ_{ij} and coordinates for each slice x^i the invariant spacetime interval becomes

$$ds^2 = (-N^2 + N^i N_i)dt^2 + 2N^i dt dx^i + \gamma_{ij} dx^i dx^j \tag{10}$$

Beyond the basic approach of 3+1 formalism lies the work in specifying the lapse and shift, evolution equation for the metric, appropriate initial conditions, defining the constraint equations from the Einstein equation, and evolving the system to extract physically meaningful quantities from the simulation. This is more difficult than it is already presented, having avoided mention of advanced numerical techniques to deal with singularities and to optimize the calculations (excision, punctures, adaptive mesh refinement.) For a more extensive and technical discussion, see [8].

While breakthroughs in numerical relativity which have allowed us to simulate black hole coalescences are relatively new, the development of numerical methods for GR date back to 1952, when Fourès-Brouhat showed the Einstein vacuum equations to be well-posed [12] (there are solutions, and initial conditions produce stable, continuous changes in the outcome.) The field developed slowly, with Hahn-Lindquist in 1964 and Smarr et al. in 1976 studying head-on collisions of non-rotating black holes with no physically meaningful results but a suspicion that meaningful results awaited more computational power. That suspicion was wrong, and it would take 30 years of developments in numerical techniques before stable, accurate simulations would be a reality. A shortlist of the work: black hole excision, BSSNOK ADM approach, GHCD treatment (constraint damping), numerical integration approaches (finite difference or spectral interpolation) and moving puncture algorithms.

Nearly coincident breakthroughs by independently working groups, each using different methods, produced the first accurate simulations of binary black hole coalescences. Pretorius [32] used the GHCD treatment and black hole excision and introduced black hole spin in initial conditions, the Brownsville [26] and GSFC [18] groups used the BSSNOK approach and moving punctures with non-spinning black holes. A more detailed summary of their results follows in later sections, but it is important to note that the three groups closely agreed with each other; a graphical comparison of their results is shown in figure 4.

Numerical relativity is a well-developed and active area in general relativity whose importance in current and future research can't be overstated. Numerical relativity can accurately produce the waveform of a merging binary through its entire life cycle, and it is the only

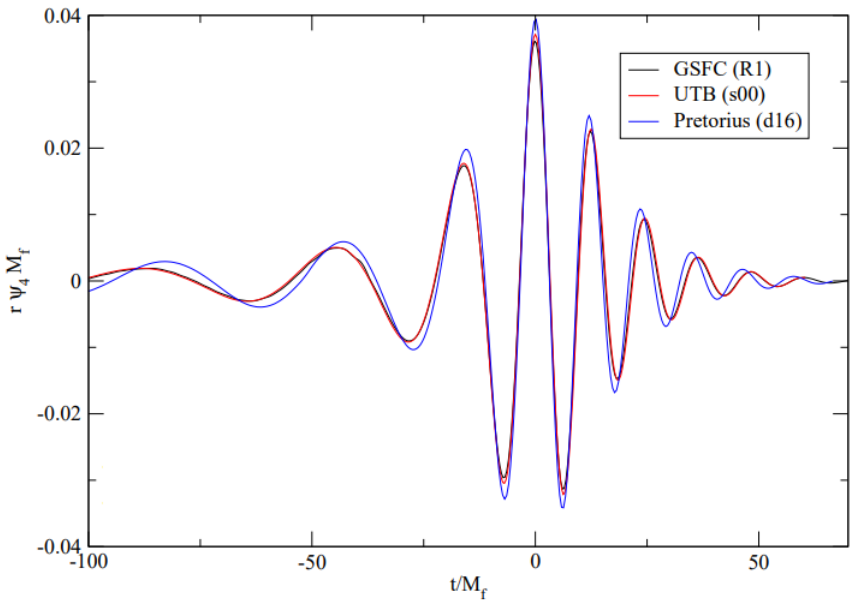

Figure 4: Comparison of waveforms generated by the three 2006 breakthrough papers in numerical relativity. GSFC and UTB used spinless black holes, Pretorius introduced a very small spin to the black holes. [19]

approach which can do so during the plunge and merger.

4 Binary Black Hole Mergers

While the focus of this paper is on spinning binary black hole systems, we turn first to simpler binary black hole systems in which individual black hole spin is zero. Since these systems share many similar properties, it is of interest to first explore these before we move on to interesting effects brought on by the black hole spin.
While these spinless systems are less complex, they are by no means simple. Whereas the two body problem in Newtonian motion is exactly solvable, there is no closed form solution to the Einstein equations for a binary system. Solving for the metric of a binary black hole system (spinning or not) would be a far more difficult task than solving for the Kerr metric proved to be. Instead, we use the approximation tools presented to model these systems to great accuracy and to draw physically meaningful quantities with which we can describe and predict their behavior and observables which we can measure like the radiation of gravitational waves, their shape and amplitude.

Black hole pairs can be formed in a number of ways, we cover here only a couple of ways this can happen [27]. They can start as a pair of stars which form together and evolve, explode and collapse into black holes (if they are massive enough.) These black holes would have co-aligned spins. Two black holes formed individually can also form a binary by capturing each other. The slingshot effect plays a crucial role in this formation; as stars passing

near black holes get slingshot away, the black hole loses some energy and drops towards the center of the cluster (dynamical friction.) This procedure eventually causes conditions in which black holes are close enough to capture each other. Once the pair is formed, their rotation can impart energy to nearby objects causing the binary to shrink and to gain enough linear momentum to escape the cluster. We expect these black holes to have randomly aligned spins. Similarly, galaxy encounter and mergers can form black hole binaries with this mechanism. Dynamical friction causes the galactic black holes to drop to the center of the merger remnant where a binary can form. Unlike the previous description, galactic centers have much stronger gravity so it's less likely the binary would escape to interstellar space.

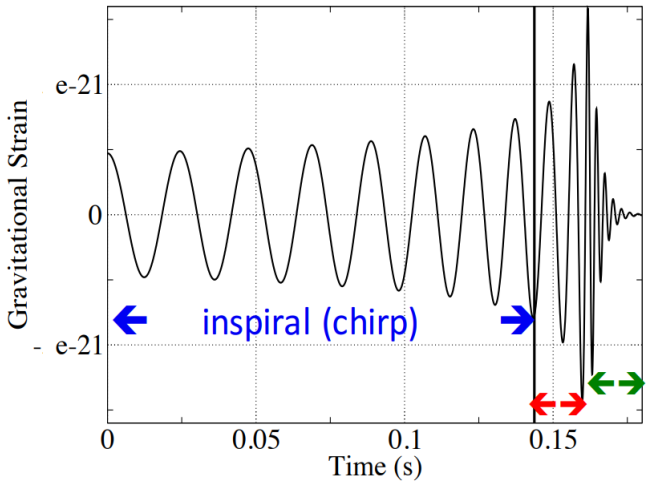

Figure 5: Strain amplitude of a binary black hole merger, with arrows pointing to the beginning and end of each phase. Inspiral, merger, and ringdown from left to right. [11]

Figure 5 shows the gravitational strain during the evolution of the system after it reaches the inspiral phase, in which the system has lost enough energy through several interaction mechanisms [27] that orbital radius decrease is mainly driven by gravitational wave radiation. From the same figure, we see that as gravitational wave radiation shrinks the orbital radius of the binary, the emitted gravitational wave increases in amplitude and frequency until it reaches a maximum at the plunge and merger (red arrows), after which it quickly settles (no hair!) into the final black hole (green arrows, ringdown). The inspiral phase is quasi-circular to good approximation [1], and it is modeled well by the Newtonian quadrupole formula. After the system reaches the innermost stable circular orbit (ISCO [6],) orbital velocities are no longer much smaller than the speed of light and tidal interactions begin to dominate, PN approximations and the quadrupole approximation break down here and numerical relativity must be used to accurately reproduce the gravitational waveform. The last part of the signal emitted by the newly formed black hole can be modeled by a superposition of damped sinusoids (the eigenfrequencies of its quasi-normal modes.)

We can gain much insight into the properties of the merger using basic physics which hold in the inspiral phase and gives results consistent with more advanced analyses [35]. By first

calculating the quadrupole moment Q_{ij} of the system's mass distribution, we can calculate the gravitational wave strain h at a luminosity distance d_L

$$h_{ij} = \frac{2G}{c^4 d_L} \frac{d^2 Q_{ij}}{dt^2} \tag{11}$$

and the rate at which energy is carried away from the system by the gravitational waves by the quadrupole formula [7][6]

$$\begin{gathered} \frac{dE_{GW}}{dt} = \frac{c^3}{16\pi G} \int\int |\dot{h}|^2 dS = \frac{1}{5} \frac{G}{c^5} \sum_{i,j=1}^{3} \frac{d^3 Q_{ij}}{dt^3} \frac{d^3 Q_{ij}}{dt^3} \\ \text{where} \qquad |\dot{h}|^2 = \sum_{i,j=1}^{3} \frac{dh_{ij}}{dt} \frac{dh_{ij}}{dt} \end{gathered} \tag{12}$$

Using Newton's laws of motion, Newton's universal law of gravitation and Einstein's quadrupole formula, we can arrive at a relation between the chirp mass of the system $\mathcal{M}$ and the gravitational wave frequency and its first derivative

$$\begin{gathered} \mathcal{M} = \frac{c^3}{G} \left(\left(\frac{5}{96} \right)^3 \pi^{-8} (f_{GW})^{-11} (\dot{f}_{GW})^3 \right)^{1/5} \\ \text{where the chirp mass is} \qquad \mathcal{M} = \frac{(m_1 m_2)^{3/5}}{(m_1 + m_2)^{1/5}} \end{gathered} \tag{13}$$

we can integrate this equation to obtain

$$f_{GW}^{-8/3}(t) = \frac{(8\pi)^{8/3}}{5} \left(\frac{G\mathcal{M}}{c^3} \right)^{5/3} (t_c - t) \tag{14}$$

where t_c is the time of coalescence. It should be noted that these numbers don't hold for all mass configurations and are otherwise limited, but they give a glimpse into the behavior of binaries in the inspiral phase. Beyond the ISCO, analytical approximations cease to serve us and we must turn to numerical relativity to continue.

In the previous section we covered the basics of numerical relativity and the work that went into reaching the first accurate waveform model of gravitational waves in 2006 [32][26][18]; figure 4 shows the waveforms generated. We will summarize their results before moving to a general discussion of the expected effects contributed by individual spins of the coalescing black holes.

Pretorius evolved black holes of equal mass and small eccentricity at different resolutions, the corotational binary model implies a small spin (a/m = 0.08) on the initial black holes. The high resolution results show a final black hole mass equal to 95% of the initial black hole masses and a spin parameter of 0.70. A calculation of the energy emitted also indicates

that roughly 5% of the initial mass is radiated.

The UTB group evolved equal mass black hole binaries from the ISCO at different resolutions. The results show final black hole with a spin parameter of 0.683 and radiated energy equivalent to roughly 3.5% of the black hole masses, in agreement with the mass losses in the remnant horizon in their simulation.

The group at the NASA Goddard Space Flight Center also modeled an inspiraling equal mass binary during the final plunge and ringdown at different resolutions. The results show radiative losses of energy of 3.4%, which agree with values calculated by the AEI by estimating radiative losses based on final black hole horizon.

5 Spinning Binary Black Hole Mergers

As we move on to binaries with individual black hole spins, we first consider the effect of initial masses and spins on the final spin of the binary black hole coalescence, with a focus on the effects of spins on the system and their consequences rather than cataloging types of mergers and their results. Reference [2] uses a phenomenological approach to estimate the final spin as a function of individual spins, masses and orbital angular momentum. The assumptions made arrive at results which agree with post-Newtonian, perturbative, and numerical approaches.

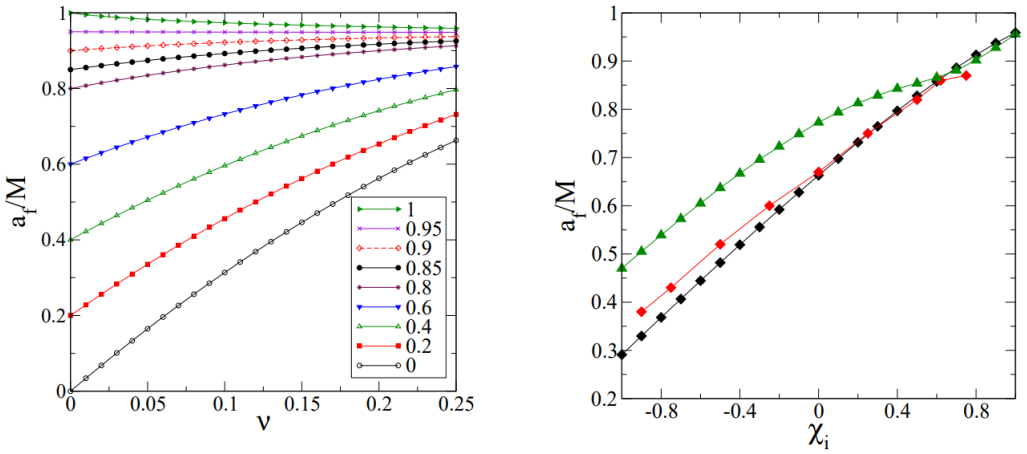

Figure 6: Estimates of the final spin of a black hole merger. On the left, final spin vs. $\nu = \frac{m_1 m_2}{(m_1+m_2)^2}$ where the equal mass case is $\nu = 0.25$. On the right, final spins vs. initial spin of equal mass black holes either aligned or anti-aligned (black); red and green traces are numerical and EOB models respectively for comparison [2]

.

For the equal spin case, figure 6 on the left panel shows the expected results. There is a critical value of 0.948 for the final spin of the merger, above which the final spin of the black

hole increases as the mass ratio decreases; it's worth noting that it is only possible to end up with a maximally spinning black hole if the initial black holes are maximally spinning and with unequal initial black hole masses [2][25]. Below this value , the spin increases as the equal mass case is reached. For non-spinning black holes, the maximum spin for the equal mass case has a value of 0.65-0.7. This agrees with the results presented in the previous page. On the right panel, the case in which spins are equal but anti-aligned is considered for equal mass binaries. Finally, consider the case in which both spins are anti-aligned with the initial orbital angular momentum. In this case, we have both spin-spin and spin-orbit interactions which can results in interesting effects (the "hangup effect," spin flips and orbital precession) and waveforms which we will discuss in later sections. Interestingly, this means that we can have a system in which the spin of the final black hole is zero when the angular momentum at the ISCO is exactly counteracted by the individual black hole spins. This scenario sits in between the cases in which the direction of the final spin is determined by the initial angular momentum of the binary, and that in which the final spin is determined by the spin of the individual black holes (this means there is an extreme case in which the final spin of the black hole opposes the initial angular momentum).

For unequal spin cases ($\chi_2 = \alpha\chi_1$, where alpha is a number from -1 to 1) with equal mass black holes, the final black hole has a maximum spin when $\chi_1 = \chi_2$, and a minimum when the initial spins are exactly opposite. Unequal mass and unequal spin binaries also give rise to an asymmetry in the emitted linear momentum from each of the black holes, once the black holes merge the linear momentum imparts a large kick to the newly formed black hole [17] (gravitational recoil,) which we also will discuss. We would also see spin-spin and spin-orbit effects as in the previous cases. The more general case of unequal spins in generic alignment will generate modulation to the observed gravitational wave signal as the orbital effects become more complex while our detectors have a limited antenna-like pattern.

5.1 The "Hangup Effect"

Spins can have a dramatic effect on the inspiral phase of the black hole merger [25][24]. When the spins are aligned with the orbital angular momentum the merger is delayed while the final separation at ISCO is smaller. The opposite happens for anti-aligned spins, a shorter merger at a larger final separation. This effect is due to a spin-orbit coupling that effectively adds repulsion when $\mathbf{S} \cdot \mathbf{L}$ is positive and attraction when it is positive, see figure 7. Due to its prolonged evolution, the aligned spin (positive $\mathbf{S} \cdot \mathbf{L}$) merger radiates more energy and produces a smaller final mass black hole than the anti-aligned or zero spin counterparts. Finally, the spin-orbit interaction of the configuration also determines final black holes spin, with the aligned merger resulting in a larger final spin magnitude and the anti-aligned case with a smaller one.

5.2 Gravitational Recoil (or gravitational "kicks")

One of the most interesting effects of spinning black hole mergers is the emission of linear momentum during the coalescence due to asymmetry in the spin or mass configuration

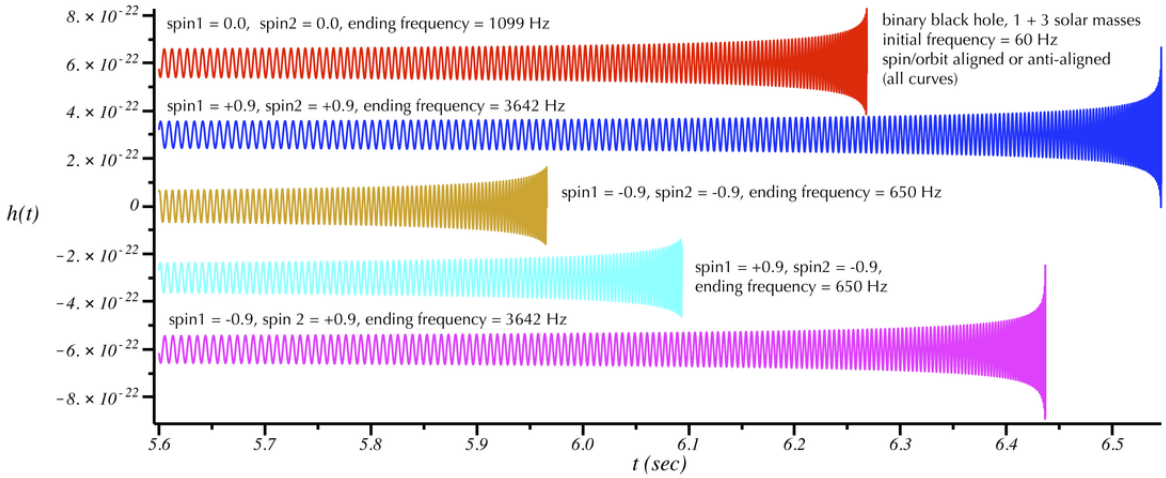

Figure 7: Gravitational wave signals from black hole binaries with different spins, and aligned or anti-aligned. Spin1 refers to a 1 solar mass black hole, spin2 refers to a 3 solar mass black hole.

of the binary. This effect accelerates (hence the names gravitational recoil or "kicks") the final black hole away from the center of mass of the original binary. A good analogy (at least for kicks in the orbital plane) is to consider an S shaped sprinkler head which shoots jets of water from each end. If the water (linear momentum) shot from each jet is equal, forces balance out to a net zero momentum imparted to the system; however, if the two jets are unequal there is a net momentum imparted to the system. An increasing flow of water (gravitational wave amplitude increase) causes the system to describe an outward spiral. If the water is suddenly cut off, the sprinkler would cost in some direction in its orbital plane. While this analogy is good, it only makes reference to the effect of non-spinning black hole binaries of unequal mass. A spinning black hole configuration can impart linear momentum when individual black hole spins point outside of the plane, even in the equal mass case [21]. A more interesting phenomenon is that of gravitational recoil out of the orbital plane when the individual spins lie in the orbital plane [28].

While gravitational kicks from spinning and non-spinning binary mergers have been studied analytically before breakthroughs in numerical relativity allowed for a full model through plunge and merger, it was considered that maximum kicks would be no larger than 500 km/s. The first simulations of non-spinning black hole binary inspirals [20] ranging in mass ratios from 1 to 0.25 calculated a maximum kick velocity of 175 km/s (for $0.3 \lesssim q \lesssim 0.4$). Simulations of equal mass spinning black hole mergers [13] with spins aligned/anti-aligned with the orbital angular momentum calculated a maximum kick velocity of 475 km/s for maximally spinning black holes. To gain some sense of scale, 300 km/s is th escape velocity from the center of dwarf elliptical galaxies. This result suggests typical kicks of 400 km/s in astrophysical black hole mergers and could explain the absence of central black holes in dwarf galaxies.

Soon, Campanelli et al [28] would publish results of generic black hole binaries, with unequal masses and misaligned spins. The results predicted that the maximum recoil velocity

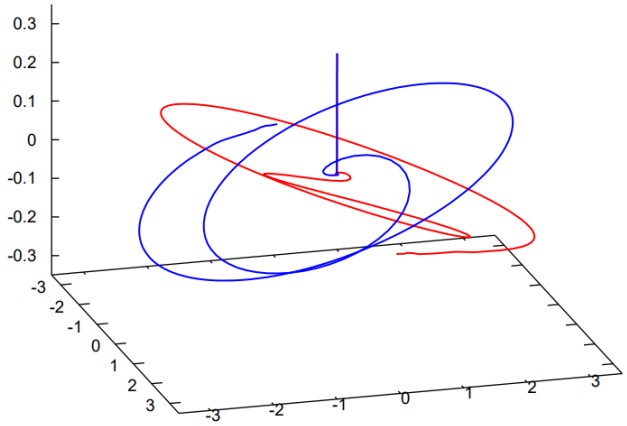

Figure 8: Three-dimensional trajectories of the punctures showing orbital precession and the final recoil for the SP2 configuration. [29]

is achieved with equal mass black holes with opposite and maximal spins lying on the orbital plane (SP2 configuration, which would be coined a "superkick" configuration.) Qualitatively, for half the orbit, the black hole spins beam gravitational radiation preferentially in the +z direction the binary recoils downward. Through the other half orbit, the opposite happens and the system recoils upward. If the merger happens during one of the swings, the final black hole receives this linear momentum and continues with that velocity. The simulation uses anti-aligned spins of a/m=$\pm$0.5 and calculated recoil velocity of 1800 km/s, rescaling to maximally spinning black holes produces a maximum recoil of 4000 km/s out of the orbital plane. Figure 8 shows the trajectory of the black holes through merger and kick. Gonzalez et al [21] would test the results reported by this configuration and report predicted velocities of 2500 km/s.

In 2011, Lousto and Zlochower would push these limits up to 5000 km/s [24], and present evidence that the greatest kicks are created by a combination of the superkick (SP2) and hangup configurations. This "hangup kick" configuration has the property that the in-plane (with the orbital angular momentum) spin component of the black holes have the same magnitude but opposite sign, and the out-of-plane spin components have the same magnitude and sign. In this configuration, the binary does not precess but rather moves up and down in the direction of orbital angular momentum.

Central escape velocities from giant elliptical galaxies spiral galaxy bulges are between 450 to 2000 km/s. The maximum kick velocities presented are large enough to easily eject the black hole remnant. However, large recoil velocities might not be frequent and there is no evidence of ejection from bulge galaxies so far. Studies also suggest that interactions with surrounding gas would tend to align the spin of the merging black holes with their orbital angular momentum [37]. Meanwhile, as mentioned before, the escape velocities for dwarf elliptical and spheroidal galaxies is below 300 km/s and well below the expected typical recoil velocities of black hole mergers.

5.3 Spin Flip

The existence of X-shaped radio galaxies has been of interest for many years, and has received a number of possible explanations among which the spin flip phenomenon hypothesis has emerged (along with increased attention) relatively recently as a leading explanation [14]. X-shaped radio galaxies exhibit two low-surface-brightness radio lobes oriented at an angle to the active high-surface-brightness radio lobes. Both lobes pass through the center of the source galaxy, suggesting a singular source for both jets. The mechanism briefly described earlier for the generation of spin flips is therefore an exciting development in astrophysics.As mentioned before, there is a boundary case in which the anti-aligned individual spins of component black holes in the binary can cancel out the orbital angular momentum of the system to create a final non-spinning black hole. This leads to both the possibility of the spin flip of the system's angular momentum due to rapidly spinning anti-aligned black holes as well the flip of the individual spins to the system's angular momentum.

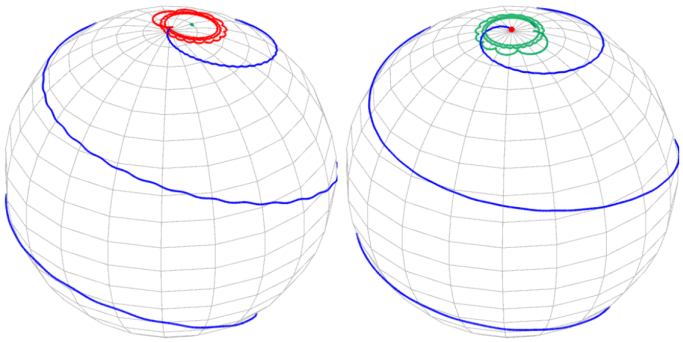

Figure 9: Directional evolutions of the spins and angular momentum of the flip flopping configuration in the initial coordinate frame (left) and in the non-inertial $\vec{L}$ frame. Colors: red $\hat{L}$, green $\hat{J}$, blue $\hat{S}_1$ [3]

We can also consider the behavior of individual spins in generic black hole configuration and highlight a recent letter which finds a flip-flopping configuration of spins [3], i.e. the precession dynamics of individual black hole spins (spin-spin effects). Figure 9 shows the evolution of this behavior, in which the spin of one of the black holes in the binary flips from aligned to the orbital angular momentum to complete anti-alignment. Post-Newtonian calculations also suggest that this behavior continues through the lifetime of the merger and would cause a small modulation of the gravitational waveform.

5.4 Precession

Through our qualitative discussion of the effects of spin on binary black hole motion, we have skimmed past the details of the precession of the spin, the angular momentum and the orbital plane. We restrict our (short) foray into the details of binary black hole precession to a timescale in which we need only consider the evolution of the precession of the spin

vectors and the orbital angular momentum. The classic Apostolatos paper produced a very thorough treatment of precession due to both spin-spin effects and and spin-orbit effects, though lengthy and beyond the level of detail offered in this paper [39]. Precession is an important effect to consider in the search for gravitational wave signals as it has the effect of modulating the amplitude and phase of the waveform as in figure 10, and development in modeling techniques and data analysis in this area continues as gravitational wave detectors improve [22].

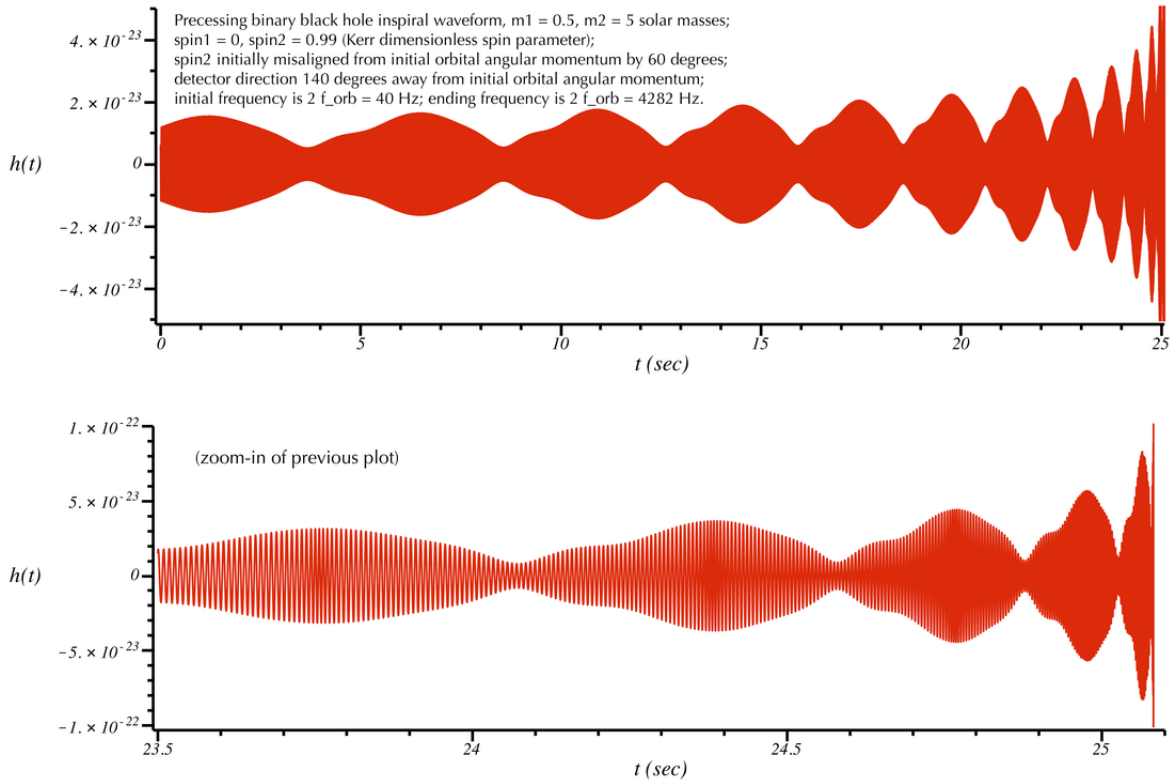

Figure 10: Based on the equations from [39], modulated signal amplitude (top) and phase (bottom) due to precession. [36]

.

We can express the equations which govern the motion of the system as a relative one-body equation of motion [40]

$$\mathbf{a} = \mathbf{a}_N + \mathbf{a}_{PN} + \mathbf{a}_{SO} + \mathbf{a}_{2PN} + \mathbf{a}_{SS} + \mathbf{a}_{RR} \tag{15}$$

Here, $\mathbf{a}_N$, $\mathbf{a}_{PN}$ and $\mathbf{a}_{2PN}$ are Newtonian and up to Post-Newtonian contributions, $\mathbf{a}_{RR}$ is a radiation reaction force, $\mathbf{a}_{SO}$ and $\mathbf{a}_{SS}$ are the spin-orbit and spin-spin interactions. Only $\mathbf{a}_{SO}$ and $\mathbf{a}_{SS}$ are not constrained to the orbital, causing a precession of the orbital plane, and resulting in modulation as in figure 10. In addition to precession of the orbital plane, the individual spin vectors exhibit precession determined by interaction with each (spin-spin coupling) other and with the orbital angular momentum (spin-orbit coupling). The spin precession equations have the form $\dot{\mathbf{S}}_i = \mathbf{\Omega}_a \times \mathbf{S}_i$; the magnitude of spin remains constant,

with a precession frequency given by $|\mathbf{\Omega}_a|$. However, if both bodies are spinning, the total spin $\mathbf{S}$ does not have a constant magnitude as the spins precess.

6 Gravitational Wave Detectors

On September 15, gravitational waves were detected using interferometric gravitational wave detectors. So far there have been 11 gravitational wave detections by LIGO. There have been many attempts at directly observing gravitational waves, beginning with resonant bar detectors (Wever, ALLEGRA) and even cosmic microwave background imaging telescopes (which also had a withdrawn claim of detected gravitational waves.) We will focus on the science gathered by the LIGO detectors, and their limitations.

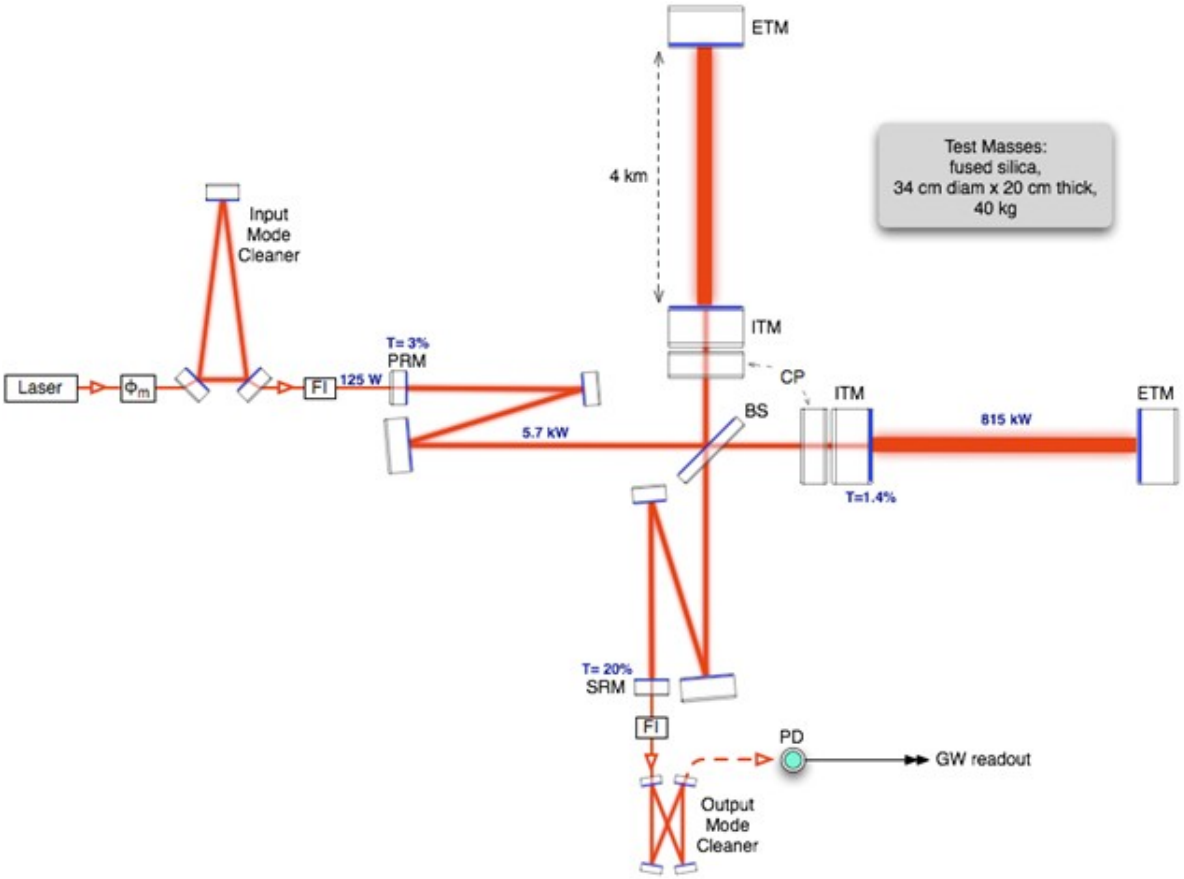

Figure 11: A detailed, though not complete, optical layout of the LIGO interferometer.

LIGO is the Laser Interferometer Gravitational-Wave Observatory, the observatory consists of two dual recycled, cavity enhanced Michelson interferometers. The current design sensitivity nears a strain of $10^{-24}m/\sqrt{Hz}$ at its most sensitive frequency. The concept of the interferometer readout scheme for gravitational wave detection is no different from the basic understanding of Michelson interferometers. Interferometry takes advantage of the superposition principle by sending a laser beam through a beam splitter, where it is split into two

beams. Each beam travels down one of the orthogonal arms, and is reflected back by a mirror at the end of the arm. Upon returning to the beam splitter both beams are recombined and are incident on a photo diode. The intensity measured by the photo diode is dependent on the phase difference the beams travel as they go down the arms. When a gravitational wave passes, it warps spacetime increasing the proper time it takes one beam to travel down on fo the arms while decreasing it in the other direction. This is an effective length change of the arm lengths and so a phase difference between the light fields recombined at the beam splitter emerges. Assuming the interferometer is set up so that in an unperturbed configuration the photo diode sees no incident light, when a gravitational wave passes the intensity measured would increase and decrease at the frequency of the gravitational wave. This description of the basic Michelson interferometer is a decent enough picture of how the LIGO detectors work; the real picture includes layers of technical advancement and improvements that allow the LIGO interferometers to be the most sensitive detectors ever built.

Ligo isn't the only interferometric detector conceived, and it is now getting ready to start its third observation run. Since before the first detections, other detectors have been built (GEO600, Virgo,) with Virgo recently helping LIGO in sky triangulation efforts and improved detection. Many more are being built (KAGRA) or conceptualized (IndiGO, Einstein Telescope, etc.;) however, LIGO is currently the only fully operational detector and the only one which has provided meaningful data.

6.1 LIGO results

Since the first LIGO detection (GW150914,) there have been ten total observations of the merger of stellar mass compact binary black holes[38] (and one binary neutron star merger with coincident and remnant electromagnetic counterparts!) LIGO has observed binary black holes with component masses which span from 7.7 to 50.6 solar masses and final black hole masses ranging from 17.8 to 80.3 solar masses. Observation distances have ranged from 40 to 2750 Mpc. The radiated energy from from all the mergers sits around 5% of the total mass of the component black holes, in agreement with numerical simulations we have covered. The medians of all final spin distributions are around 0.7. The component spins seem to favor either small magnitude spins or spins which tend to be tilted into the orbital plane, future work and improvements in sensitivity will improve our understanding of component spin and the information it can provide about black hole binary formation. Currently, LIGO isn't able to constrain meaningfully the spin of the component black holes. LIGO searches also don't consider precession effects at the moment.

6.2 Why doesn't LIGO see individual spins?

The answer in short reduces to "with our current detector sensitivity it is difficult to measure the spins of individual black holes" [5]. While LIGO observations have been able to place an upper constrain on the individual spins of component black holes, it has proven difficult to go beyond as spin effects couple to the gravitational waveform in ways similar to

that of component masses and mass ratios. The collaboration instead uses another parameter, the effective aligned spin χ_{eff}, to characterize (to some extent) the spin components of the binary.

$$\chi_{eff} = \frac{(m_1\vec{\chi}_1 + m_2\vec{\chi}_2) \cdot \hat{L}_N}{(m_1 + m_2)} \qquad \text{where} \quad \hat{L} = \hat{L}_N \qquad \text{for aligned spin binaries} \tag{16}$$

The distribution of the effective spin in LIGO observations so far is mostly distributed around 0 (see table 1,) with the exception of GW170729 and GW151226 for which the spins are non-zero within a 90% confidence range.

GW150914	GW151012	GW151226	GW170104	GW170608	GW170729	GW170809	GW170814	GW170818	GW170823
$-0.01^{+0.12}_{-0.13}$	$0.04^{+0.28}_{-0.19}$	$0.18^{+0.20}_{-0.12}$	$-0.04^{+0.17}_{-0.20}$	$0.03^{+0.19}_{-0.07}$	$0.36^{+0.21}_{-0.25}$	$0.07^{+0.16}_{-0.16}$	$0.07^{+0.12}_{-0.11}$	$-0.09^{+0.18}_{-0.21}$	$0.08^{+0.20}_{-0.22}$

Table 1: Effective spin for all LIGO observations. [38]

It's important to understand χ_{eff} is not a measure of individual spins but rather a measure of combined spin which is aligned to the orbital angular moment of the binary. A positive χ_{eff} suggests that both spins are aligned whereas a negative χ_{eff} suggests spins are anti-aligned. It does give us a physical observation of orbital hangup, described before.

A detailed numerical investigation of LIGO's ability to measure black hole spins from observations is not likely below an SNR of $\mathcal{O}(1000)$ for low mass binaries or 100 for higher masses[30]. LIGO's current highest observed SNR is 9.7.

7 Conclusion

In theory, black holes are simple objects described only by its mass and spin. However, their interactions are much more complex and incredibly hard to measure. Black hole mergers are one of the most powerful astronomical events, and one of the most difficult to observer and understand. With ten black hole detection under its belt, LIGO is leading the path to gravitational wave astronomy. As the numbers grow and the statistical analysis of black hole mergers improves, our knowledge of the formation of black holes and our cosmos expands. LIGO has plans beyond the next observation run (LIGO A+) and the scientific community has plans for interferometers beyond LIGO in the coming decades (LISA, ET, Voyager, Kagra) so that we will, in the near future, have the tools to see the details which are not in reach now.

References

[1] Gregory B. Cook Alessandra Buonanno and Frans Pretorius. Inspiral, merger, and ring-down of equal-mass black-hole binaries. *Phys. Rev. D*, 75:124018, 2007.

[2] Luis Lehner Alessandra Buonanno, Lawrence E. Kidder. Estimating the final spin of a binary black hole coalescence. *Phys.Rev.D*, 77:026004, 2008.

[3] James Healy Carlos O. Lousto. Flip-flopping binary black holes. *PhysRevLett*, 114:141101, 2015.

[4] Cecilia Chirenti. Black hole quasinormal modes in the era of ligo, 2017.

[5] LIGO Scientific Collaboration. Gwtc-1: A new catalog of gravitational-wave detections, 2018.

[6] JA Wheeler CW Misner, KS Thorne. *Gravitation*. 1975.

[7] A. Einstein. Sitzungsberichte der koniglich preussis-chen. *Akademie der Wissenschaften (Berlin)*, pages 154–167, 1918.

[8] Robert A. Eisenstein. Numerical relativity and the discovery of gravitational waves, 2018.

[9] B. P. Abbott et al. Observation of gravitational waves from a binary black hole merger. *Phys. Rev. Lett.*, 116:061102, 2016.

[10] Francis Everitt et al. Gravity probe B experiment, science results - NASA final report, 2008.

[11] Valeria Ferrari. Black holes, white dwarfs, and neutron stars: The physics of compact objects.

[12] Y. Fourès-Bruhat. Theoreme d'existence pour certains systemes d'equations aux derivees partielles non lineaires. *Acta Math.*, 88:141–225, 1952.

[13] Deirdre Shoemaker Pablo Laguna Frank Herrmann, Ian Hinder. Gravitational recoil from spinning binary black hole mergers. *Astrophys.J.*, 661:430.

[14] Laszlo A. Gergely Gopal-Krishna, Peter L. Biermann and Paul J. Wiita. On the origin of x-shaped radio galaxies. *Research in Astron. Astrophys*, 12-2:127.

[15] Eric Gourgoulhon. 3+1 formalism and bases of numerical relativity, 2007.

[16] Werner Israel. Event horizons in static vacuum space-times. *Phys. Rev.*, 164:1776, 1967.

[17] Ian Ruchlin James Healy, Carlos O. Lousto and Yosef Zlochower. Evolutions of unequal mass, highly spinning black hole binaries. *PhysRevD*, 97:104026, 2018.

[18] Dae-Il Choi Michael Koppitz John G. Baker, Joan Centrella and James van Meter. Gravitational-wave extraction from an inspiraling configuration of merging black holes. *Phys. Rev. Lett.*, 96:111102, 2006.

[19] Frans Pretorius John G. Baker, Manuela Campanelli and Yosef Zlochower. Comparisons of binary black hole merger waveforms. *Class. Quant. Grav.*, 24:S25–S31, 2007.

[20] Bernd Brugmann Mark Hannam Jose A. Gonzalez, Ulrich Sperhake and Sascha Husa. Maximum kick from nonspinning black-hole binary inspiral. *Phys. Rev. Lett.*, 98:091101, 2007.

[21] Ulrich Sperhake Bernd Brugmann Sascha Husa Jose A. Gonzalez, Mark Hannam. Supermassive recoil velocities for binary black-hole mergers with antialigned spins. *PhysRevLett*, 98:231101, 2007.

[22] Neil Cornish Nicolas Yunes Katerina Chatziioannou, Antoine Klein. Analytic gravitational waveforms for generic precessing compact binaries. *Phys. Rev. Lett.*, 118:051101, 2017.

[23] Roy P. Kerr. Gravitational field of a spinning mass as an example of algebraically special metrics. *Phys. Rev. Lett.*, 11:237, 1963.

[24] C. O. Lousto and Y. Zlochower. Hangup kicks: Still larger recoils by partial spin/orbit alignment of black-hole binaries. *Phys. Rev. Lett.*, 107:231102, 2011.

[25] C. O. Lousto M. Campanelli and Y. Zlochower. Spinning-black-hole binaries: The orbital hang up. *Phys.Rev.D*, 74:041501, 2006.

[26] P. Marronetti M. Campanelli, C. O. Lousto and Y. Zlochower. Accurate evolutions of orbiting black-hole binaries without excision. *Phys. Rev. Lett.*, 96:111101, 2006.

[27] A. Sesana M. Mapelli M. Celoria, R. Oliveri. Lecture notes on black hole binary astrophysics, 2018.

[28] Yosef Zlochower Manuela Campanelli, Carlos Lousto and David Merritt. Large merger recoils and spin flips from generic black-hole binaries. *Astrophyisics.J.*, 659:L5–L8, 2007.

[29] Yosef Zlochower Manuela Campanelli, Carlos O. Lousto and David Merritt. Maximum gravitational recoil. *Phys.Rev.Lett.*, 98:231102, 2007.

[30] Mark Hannam Michael Purrer and Frank Ohme. Can we measure individual black-hole spins from gravitational-wave observations? *Phys. Rev. D*, 93:084042, 2016.

[31] Eric Poisson and Clifford M. Will. *Gravity: Newtonian, Post-Newtonian, Relativistic.* 2014.

[32] Frans Pretorius. Evolution of binary black-hole spacetimes. *Phys. Rev. Lett., volume=95, pages=121101, year=2005.*

[33] C. W. Misner R. Arnowitt, S. Deser. Gravitation: an introduction to current research. *Lous Witten ed.*, Chapter 7:227–265, 1962.

[34] Karl Schwarzschild. Über das gravitationsfeld eines massenpunktes nach der einsteinschen theorie. *Sitzungsberichte der Königlich Preußischen Akademie der Wissenschaften (Berlin)*, pages 189–196, 1916.

[35] LIGO Scientific and VIRGO Collaborations. The basic physics of the binary black hole merger gw150914. *Ann. Phys. (Berlin)*, 529:1–2, 2017.

[36] soundsofspacetime.org. Spinning binaries, exploring spin and precession, 2018.

[37] Christopher S. Reynolds Tamara Bogdanovic and M. Coleman Miller. Alignment of the spins of supermassive black holes prior to coalescence. *The Astrophysical Journal*, 661:L147–L150, 2007.

[38] the Virgo Collaboration The LIGO Scientific Collaboration. Gwtc-1: A gravitational-wave transient catalog of compact binary mergers observed by ligo and virgo during the first and second observing runs. *LIGO-P1800307*, 2018.

[39] Gerald J. Sussman Theocharis A. Apostolatos, Curt Cutler and Kip S. Thorne. Spin-induced orbital precession and its modulation of the gravitational waveforms from merging binaries. *Physical Review D*, 49:6274, 1994.

[40] Kip S. Thorne and James B. Hartle. Laws of motion and precession for black holes and other bodies. *Phys. Rev. D*, 31:1815, 1985.

[41] Matt Visser. The kerr spacetime: A brief introduction, 2007.